Indonesian Journal of Science & Technology

Journal homepage: http://ejournal.upi.edu/index.php/ijost/

Toxic heavy metals removal using a hydroxyapatite and hydroxyethyl cellulose modified with a new Gum Arabic

A. Errich[1], K. Azzaoui[2], E. Mejdoubi[2], B. Hammouti[2*], N. Abidi[3], N. Akartasse[2], L. Benidire[4], S. EL Hajjaji[1], R. Sabbahi[4], A. Lamhamdi[2,5]*

[1]Mohamed V University, Rabat Agdal, Morocco
[2] Mohammed Premier University, Morocco
[3]Texas Tech University, Lubbock, TX, United States
[4]Ibn Zohr University, Morocco
[5]Abdelmalek Essaadi University, Morocco
Correspondence E-mail: hammoutib@gmail.com and k.azzaoui@yahoo.com

ABSTRACTS

The objective of this work was to develop a process that allows the synthesis of an apatitic material of controlled composition and morphology, which could be used for medical and environmental applications. The adsorbent was synthesized, and characterized using scanning electron microscopy, nuclear magnetic resonance, Thermal analysis and other techniques, Atomic Force Microscopy, X-ray photoelectron spectroscopy and Total organic carbon. Different experimental parameters such as the effect of the amount of adsorbent, solution pH and temperatures and contact times were studied. Pseudo-order kinetics models were studied, and our data followed a pseudo second order. Experimental data were analyzed for both Langmuir and Freundlich models and the data fitted well with the Langmuir isotherm model. To understand the mechanism of adsorption, thermodynamic parameters like standard enthalpy, standard Gibbs free energy, and standard entropy were studied. The study indicated that the process is spontaneous, exothermic in nature and follow physisorption mechanisms. The novelty of this study showed surface of composite based of hydroxyapatite has the ability to highlight the surface designed for efficient removal of Cu^{2+} and Zn^{2+} ions, from aqueous solutions more than other studies.

ARTICLE INFO

Article History:
Received 07 Oct 2020
Revised 28 Nov 2020
Accepted 03 Dec 2020
Available online 20 Jan 2021

Keywords:
Composite,
Hydroxyethylecellulose,
Hydroxyapatite,
Gum Arabic,
Nanostructure,
Adsorption.

1. INTRODUCTION

Heavy metal ions released into the environment from a variety of industrial processes are an indisputable problem (Hamed *et al.,* 2019; Tabaght *et al* 2019). Long term exposure of heavy metals may cause serious damage to liver, kidney, lung problem (Dhillon *et al*., 2016). Long term exposure of heavy metals may cause serious damage to liver, kidney, lung cancer, reduction in hemoglobin formation, emphysema, hypertension, and testicular atrophy diseases, etc (Dhillon *et al*., 2017). Zinc, and Copper for example, are well-known as dangerous elements for human health even at very low concentrations, and their concentration in the environment should be kept under permanent control. For humans, the main sources of these metals are water and food, so rapid and sensitive methods must be accessible for their determination in these samples (Dhillon *et al*., 2017).

Monodisperse chitosan-bound Fe_3O_4 nanoparticles were developed to efficiently remove Cu^{2+} ions (Destainville *et al*., 2003). The adsorbent exhibited a maximum Langmuir adsorption capacity of 21.5 mg/g. Banerjee and Chen compared the adsorption of Cu^{2+} onto magnetic nanoparticles (Fe_3O_4) and magnetic nanoparticles treated with Gum Arabic (Gandhi *et al*., 2011). It was found that the adsorption capacity of modified nanoparticles with Gum Arabic was higher (38.5mg/g) compared to the pristine nanoparticles (17.6 mg/g). This higher adsorption capacity was attributed to the carboxylic groups of gum arabic, the complexation of the amine group of gum arabic, and the surface hydroxyl groups of iron oxide.

Also, the performance of chitosan/ hydroxyapatite (Cs/HAp) composite nanofiber membrane prepared by electrospinning process for the removal of lead, cobalt and nickel ions from aqueous solution has been demonstrated (Aliabadi *et al.,* 2014).

Several studies were focused on using hydroxyapatite (HAp) of different origins to remove zinc ions from the solution (Pivarciova *et al.,* 2014). showed that the adsorption of zinc on HApwas pH independent ranging from 4.5 to 6.5 as a result of the buffering properties of the HAp(Lee *et al*., 2005). Work on zinc sorption is often contradictory or complementary. Some authors consider that the sorption mechanisms are close to those of cadmium (ion exchange), in relation to their ionic ratios. Others highlighted the formation of new highly crystalline phases charged with zinc (Lee *et al.,* 2005). reported that for initial low zinc concentrations (<49 ppm), the formation of zinc precipitate does not occur (Pivarciova *et al*., 2014). However, for higher concentrations (> 49 ppm), the presence of Hopeite $Zn_3(PO_4)_2$, $4H_2O$ was detected under acidic conditions, whereas under alkaline conditions, the formation of ZnO and hydrozincite $Zn_5(OH)_6(CO_3)_2$ was favored (Pivarciova *et al*., 2014).

Investigated the sorption of different metals (Cd, Zn, Cu, Pb) by synthetic calcium hydroxyapatite (Ca-Hap) as monometallic, bimetallic, and multi-metallic systems (Corami *et al*., 2007). In the case of mono-metallic studies, the fixation of Zn and Cu was explained by a rapid surface complexation step followed by a partial dissolution of Ca-HAp and ion exchange with Ca. The result would be the formation of a new phase of Ca-HAp loaded in ML, of the gross formula $ML_xCa_{10-x}(PO_4)_6(OH)_2$. The characterization by DRX and SEM did not allow the detection and identification of new phases after sorption or morphological change. Nevertheless, analysis confirmed the presence of MLs on the surface. In their latest study, characterization by Extended X-Ray Absorption Fine Structure structural analysis

DOI: https://doi.org/10.17509/ijost.v6i1.31480 |
p- ISSN 2528-1410 e- ISSN 2527-8045 |

on Cu-doped Ca-HAp revealed the presence of Cu at Ca(II) Ca-HAp sites with a significantly decreased interatomic distance which the authors linked to a relaxation effect due to the difference between the ionic rays of Ca^{2+} (0.99 Å) and Cu^{2+} (0.73 Å) ions (Corami *et al.*, 2008). Qualitatively, the spectra show a single coordination peak corresponding to the Cu-O bond. The non modification of the structure of the apatite charged with Cu, led the authors to conclude that the metal sorption occurs at the surface sites by substitution of H^{+} ions (surface complexation at ≡POH) and Ca^{2+} ions (ion exchange with formation of a Ca-HAp charged with Cu), with a low probability of Cu binding to Ca sites of the internal structure of the crystal.

In industrialized countries, metal contamination is considered one of the most pervasive and complex environmental problems (Dhillon *et al.*, 2017). The search for solid matrices capable of trapping these pollutants is necessary (Grossl *et al.*, 1997). For this purpose, we synthesized the HAp / HEC / GA matrix having a large specific surface area for use as a material for removing Cu^{2+} and Zn^{2+} ions contained in aqueous solutions. The synthesis of HAp is influenced by several parameters which can affect the formation of HAp/HEC/GA composites (Goldberg, 1985). Nanoparticles of specific size and morphology can be easily synthesized by various methods such as coprecipitation (Gao & Mucci, 2001), hydrothermal, sol-gel (Gao & Mucci, 2001 & Goldberg & Johnstony, 2001), double decomposition method, reverse microemulsion and matrix-assisted synthesis (Jain *et al.*, 1999; Xiaoguang, *et al.*, 2005).

HAp is the best-known calcium phosphate compound. Its chemical formula is $Ca_{10}(PO_4)_6(OH)_2$ and is considered to be the most stable and the least soluble phase among calcium phosphates (Lamhamdi *et al.*, 2014). HAp belongs to the apatite family. It is theoretically composed of 39.68% Ca, 18.45% P, with a mass ratio Ca / P of 2.151 and a molar ratio of 1.667. the space group of HAp P6 3 / m **Figure 1** with the following crystallographic parameters: a = 9.418 Å; c = 6.881 Å and□□ = 120 Å (Chen *et al.*, 2008; Li *et al.*, 2004). HAphas been widely used because of its high adsorption and exchange capacities as a material capable of immobilizing various heavy metals such as Iron, Zinc, Cadmium, Copper and Lead for example (Banerjeea *et al.*, 2008), and various toxic organic molecules such as dyes and pesticides (Carabantee *et al.*, 2009; Sandip *et al.*, 2013) **Figure 1**.

The HAp is synthesized using a precipitation reaction, by adding a dibasic ammonium phosphate solution to a solution of calcium nitrate tetrahydrated at 70°C at a pH between 8.0 and 9.5 (Luong *et al.*, 2008). The zeta potential makes it possible to study the surface charge of the hydroxyapatite. The presence of PO_4^{3-} and Ca_{2+} ions plays an important role in the changes in the charge polarity and determination of the zeta potential (Zhang & Gonsalves *et al.*, 1997). Therefore, the solubility of the HAp is a function of certain physicochemical parameters, such as temperature, pH, and the nature of the adsorbed ions (Yen *et al.*, 2002). HAp has a very large capacity for removal of divalent heavy metal ions through the exchange between Ca^{2+} ions that exist in the HApstructure and heavy metal ions dissolved in water at room temperature (Elliott et al , 1973).

Gum arabic (GA) is a branched polysaccharide complex **Figure 2**, which is in a mixed salt form of Ca^{2+}, Mg^{2+}, and K^{+}. The backbone is composed of 1,3 β-D-galactopyranosyl. The side chains are composed of two to five compounds of 1,3 β-D-galactopyranosyl and are joined to the main chain by links 1, 6. The Gum Arabic is used in pharmaceutical, cosmetic and food industries as an emulsifier and stabilizer, and in some countries for traditional treatment of patients with chronic kidney disease (Elliott et al, 1973).

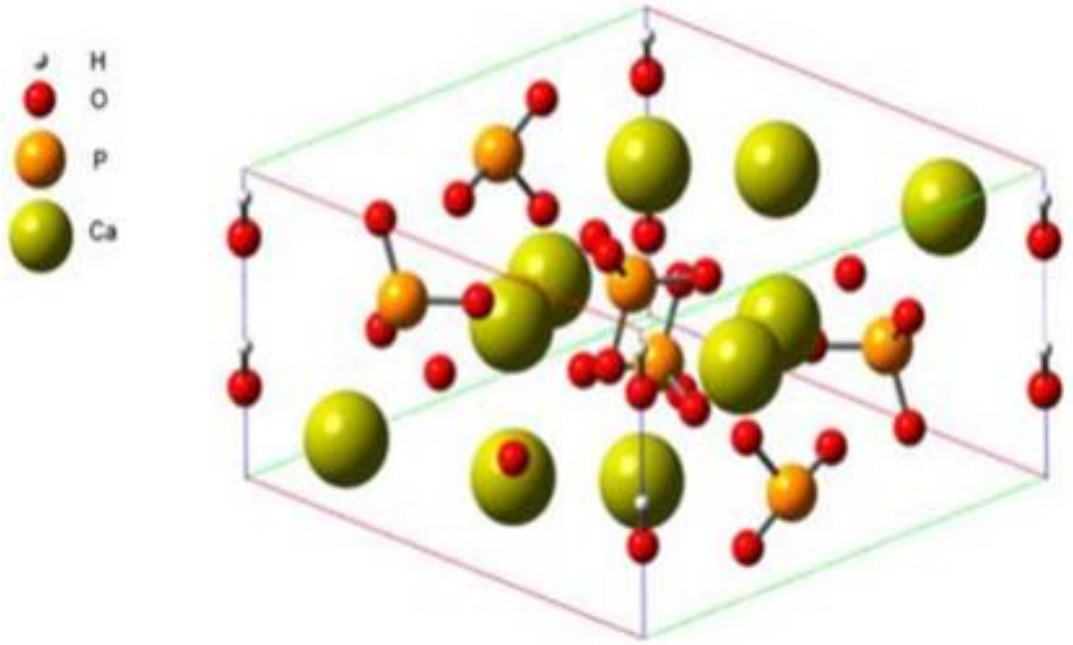

Figure 1. Crystallographic structure of HAp(Lamhamdi *et al*., 2014), published results for clinical examinations.

Figure 2. Gum arabic (GA)

The chemical structure of gum arabic is represented by a 1,3 β-D-galactopyranosyl backbone, the side chains contain α-L-arab in of uranosyl, α-L-rhamnopyranosyl, β-Dglucopyranosyl and β-4-O-methyl-D - glucopyranosyl **Figure 3**.

The gum is slightly acidic, yellowish in color, insoluble in chloroform and acetone, but soluble in water and ethanol (Takeuchi

DOI: https://doi.org/10.17509/ijost.v6i1.31480 |
p- ISSN 2528-1410 e- ISSN 2527-8045 |

et al 1988). Gum arabic is an exudate that is produced from the stems and branches of trees. The main source of GA is Sudan while other important sources include Chad, Senegal, and Nigeria. Acacia Senegal and seyal develop widely in the Sahel belt of Africa. Because of its chemical properties (stabilizer, emulsifier, etc.), Gum Arabic is used in many industrial applications, including food and pharmaceutical industries. The Gum Arabic can be considered as an arabinogalactan complex protein (AGP). One of the most interesting features of Gum Arabic is that it has similarities with extracellular matrix proteins and may be helpful to improve the behavior of bio-ceramics (Azzoui *et al*., 2015).

HAp-based composites are biomaterials used in several studies, especially for the removal of heavy metals (Banerjee & Chen, 2007). is largely applied for protein purification and in the improvement of materials to repair damaged bone (Eddy *et al*., 2014). It is also a porous carrier, natural or synthetic, biocompatible, bioactive, and osteoconductive. HApis the main mineral component of teeth and bones. It can accept an anionic and cationic substitution series in its structure because of its high affinity for the removal of heavy metals (Roque & Wilson, 2008; Lamm *et al*, 2004). HAp (Ca10 (PO4)6(OH)2) has been used in hard tissue engineering because of its excellent bioactivity, biocompatibility, and osteoconductivity. However, the use of HAp is limited by its poor mechanical properties, for example low flexural strength and low tensile strength (Kmita *et al*., 2006). Furthermore, the sorption capacity of HAp is limited by the number of sites available. To increase the retention capacity, it is necessary to explore the use of materials having a chemical affinity to associate them with HAp such as gum Arabic. Gum Arabic is a polysaccharide compound that could play a very important role in the elimination of metals given its high affinity with HAp.

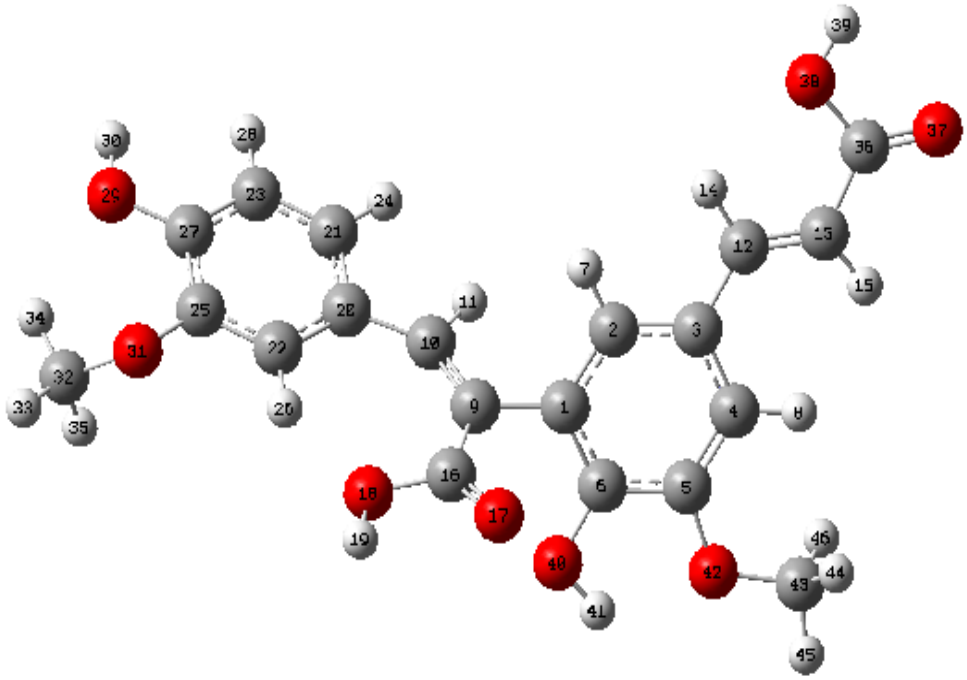

Figure 3. Spatial chemical structure of gum arabic (Elliott *et al*., 1973).

Literature shown that Glucose-6-phosphate, which is formed in this process, is used to produce cellulose by Acetobacter xylinum (Sulastri and Rahmidar, 2016). The Gum acacia, also known as gum Arabic, is an edible polysaccharide used in the food, pharmaceutical, cosmetic and textile industries, as an emulsifying, suspending and stabilizing agent. The GA of the southern region of Morocco, Laayoune-Smara, is a branched chain, a complex polysaccharide, either neutral or slightly acidic, as a mixed salt of calcium, magnesium and potassium of a polysaccharide acid. The backbone is composed of 1,3 β-linked-D-galactopyranosyl units. The side chains are composed of two to 1,3-β-linked D-galactopyranosyl units, connected to the main chain by links 1, 6. Acacia gum (GA) is used in pharmaceutical, cosmetic and as an emulsifier and a stabilizer, and in some countries, in the traditional treatment of patients with chronic kidney disease (CKD).

2. METHODS AND MATERIALS

2.1 Chemicals

The reagents and solvents used in this work were acquired from Aldrich and used without further purification. The reagents include: calcium nitrate ($Ca(NO_3)_2{\cdot}4H_2O$, 99%) and ammonium hydrogen phosphate ($(NH_4)_2{\cdot}HPO_4$, 99%). Distilled water was used in all experiments. Gum Arabic and HEC were extracted from Esparto STIPA Laayoune, Morocco.

2.2 Preparation of nanocomposite based of HAp/ HEC/ GA

The HAp/HEC/GA composites were synthesized by reacting HEC and GA with HAp in an aqueous medium. First, di-ammonium phosphate $(NH_4)_2HPO_4$ was dissolved in distilled water at T= 25°C and then the pH was adjusted to 10.5 using ammonia solution (NH_4OH). The mixture was transferred to a three-necked flask and heated to 85°C with continuous stirring. The desired amounts of $Ca(NO_3)_2.4H_2O$, GA, and HEC were separately dissolved in distilled water. The amount of GA and HEC were introduced in varying proportions in the solution of calcium nitrate. Upon homogenization of the calcium and HEC/GA solution, the resulting solution was added dropwise to the phosphate solution. The pH was adjusted to 9.5. The reaction mixture was stirred for 30 min. The precipitate obtained was filtered, washed with distilled water and then dried at 50°C for 12 h (Lamhamdi, 2014; Azzaoui *et al*, 2017).

2.3 Characterization

2.3.1 FTIR measurements

FTIR spectroscopy was performed using a Shimadzu FT-IR 300 series instrument (Shimadzu Scientific Instruments) in the region of 4000-400 cm-1 with 2 cm-1 resolution and 10 scans. Pellets were prepared by mixing 0.98 g of the nanocomposite with 0.02 g of KBr.

2.3.2 Morphological studies

Emission-scanning electron microscopy (SEM) was used to investigate the morphology of the different types of materials and the filler/matrix interface using an SU 8020, 3.0 KV SE(U). The specimens were frozen in liquid nitrogen, fractured, mounted, coated with gold/palladium, and observed using an applied tension of 10 kV.

2.3.3 XRD measurements

Composite based of Hap were analyzed using X-ray diffraction technique by means of using PHI ACESS ESCA-V6.0F software and processed using MultiPak 8.2 B package. The study was carried out to characterize phase compositions of the composite.

2.3.4 Thermogravimetric analysis

Standard thermogravimetric analyzer from TA Instrument (TGA Q500 and Q50),

DOI: https://doi.org/10.17509/ijost.v6i1.31480 |
p- ISSN 2528-1410 e- ISSN 2527-8045 |

with a temperature range of 20–900°C at a heating rate of 10°C/min was used. Differential scanning calorimetry (DSC) curves were recorded on a DSC Q2000 V24.4 Build 116. Samples (~ 10 mg) were sealed in aluminum DSC pans and placed in the DSC cell.

2.3.5 Total organic carbon

The total organic carbon (TOC) assessment (TOC/TN Analyzer multi N/C 2100/2100) was used. in place of the total organic carbon (TOC), the total carbon (TC) was used to indicate the carbon content in the aqueous effluent, as this measure accounts all carbon (organic and inorganic) that exist in the aqueous phase, which is required to establish the carbon balance. AnalytikJena AG (Germany), multi N / C and multi N / C are registered trademarks of Analytik-Jena AG.

2.3.6 Atomic force microscopy (AFM)

Atomic Force Microscopy (AFM) measurements were carried out using VEECO CPII atomic force microscope to investigate changes of the surface morphology.

2.3.7 X-ray photoelectron spectroscopy

X-ray photoelectron spectroscopy (XPS) studies were performed on a Physical Electronic PHI 5700 spectrometer using non-monochromatic Mg-Ka radiation (300 W, 15 kV and 1253.6 eV) for analyzing the core-level signals of the elements of interest with a hemispherical multichannel detector. The sample spectra were recorded with a constant pass energy value at 29.35 eV, using a 720 µm diameter circular analysis area.

2.3.8 ^{31}P NMR spectroscopy

Solid state ^{31}P Nuclear Magnetic Resonance (NMR) spectra were acquired using high-resolution magic-angle spinning (MAS) Bruker DRX-500 MHz spectrometer with 4 mm CP/MAS probe.

3. RESULTS AND DISCUSSION

3.1 FT-IR analysis

Figure 4 shows the experimental IR spectra of HAp, HEC, GA and HAp/HEC/AG composites. The IR band at 1600 cm^{-1} is assigned to the carbonyl group (C=O) vibrations. Furthermore, the CH vibrations of the three composites are located between 2950-2800 cm^{-1}. The infrared region between 1200 and 1000 cm^{-1} corresponds to the stretching vibrations of lateral groups (C-OH) and the glycosidic vibration (COC) (Lin *et al.*, 2010). The symmetrical stretching vibrations of COO^- functional group are located between 1450-1400 cm^{-1} (Kamnev *et al.*, 1988). Moreover, the C-H bands of CH_3 are observed at 2929 cm^{-1} and 2849 cm^{-1}. The FTIR band at 3335 cm^{-1} is assigned to OH^- ion vibrations. The IR vibrations of HEC are in a good agreement with the literature. This confirms the structure of the HEC extracted from Alfa of the South.

In the IR spectrum of Hap, the vibrations assigned to PO_4^{3-} and OH^- can easily be detected **Figure 4**. The vibration assigned to PO43- is characterized by the vibrations between 1100 - 900 cm-1 (assigned to P-O symmetrical and asymmetrical vibrations) and 600-500 cm-1 (assigned to O-P-O deformation) (Destainville *et al.*, 2003). When the temperature of the calcination reaction increased, it was observed that the vibrations of the PO43- are shifted to lower frequencies, which could be attributed to changes the structural order and crystallization of the solids. The characteristic vibrations of the OH of the apatite are located at 3560 and 630 cm^{-1}. However, the structural resolution of these bands depends either on the reaction temperature or the temperature of the calcination. A good resolution of these bands was observed for a calcination temperature at 900°C. These results are in good agreement with those obtained by XRD (Azzaoui *et al.*, 2017).

The IR spectra of HAp/HEC/GA composites with different mass ratios

(100/0/0; 80/10/10; 70/20/10; 60/30/10) show vibrations at 1100 cm-1 and 3500 cm-1, which are assigned to PO_4^{3-} and hydroxyl vibrations of apatite structure **Figure 4**. Furthermore, the CH vibrations for the three composites are located between 2800 and 2950 cm-1. The comparison between the three FTIR spectra indicates a change of the vibration of the alkyl group, located at 2850 cm^{-1}. This vibration is observed at 2850 cm^{-1} for the three composites a, b, and c (HAp/ HEC/ GA: 10/40/50, 60/30/10 and 70/20/10) respectively. However, the IR band of the composite 80/10/10 is observed at 2950 cm-1. In addition, the hydroxyl OH- ions band is observed between 3300 and 3600 cm^{-1}.

The morphological changes caused by GA could be due to the presence of numerous ether bonds (-O-). The stereochemical structure of pectin in the absence of water or in aqueous solution, and the process of possible formation of HAp / HEC, in the presence of GA, are shown in **Figure 5** (using Advanced Chemistry Development (ACD)/ ChemSketch software). Therefore, when GA is dissolved in aqueous solution, a GA-OH bond is formed. The GA molecule with the ability to chelate calcium ions provides the property of controlling the morphology of the formed compound grains (Gopi *et al*., 2015). GA has three important properties; modifies the surface of the apatite crystal; controls the reaction rate; and finally, acts as a dispersant of apatite particles. In aqueous solution, the flexibility of GA molecules increased when the temperature increased. Therefore, the synthesis at high temperature, the development of HApcrystals will be oriented by the strong flexible GA molecules. This would lead to the formation of large HApplatelets. On the other hand, at a low temperature, the weak flexible colloids of polyethylene glycol should be responsible for the formation of a small size HApparticles. The stereochemical structure of polyethylene glycol in the absence of water or in aqueous solution and the process of possible formation of HAp/HEC in the presence of GA are shown **Figure 6** (using Advanced Chemistry Development (ACD)/ChemSketch software).

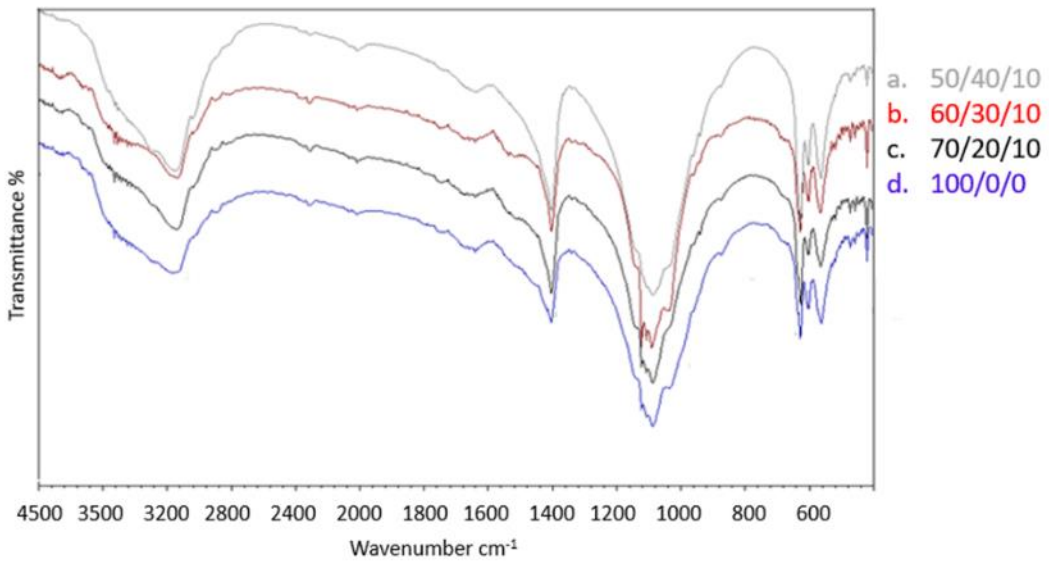

Figure 4. FTIR spectra of HAp, HEC and composite based of HAp/ HEC/ GA: (a) 50/40/10, (b) 60/30/20, (c) 70/20/10, and (d) 100/0/0.

DOI: https://doi.org/10.17509/ijost.v6i1.31480 |
p- ISSN 2528-1410 e- ISSN 2527-8045 |

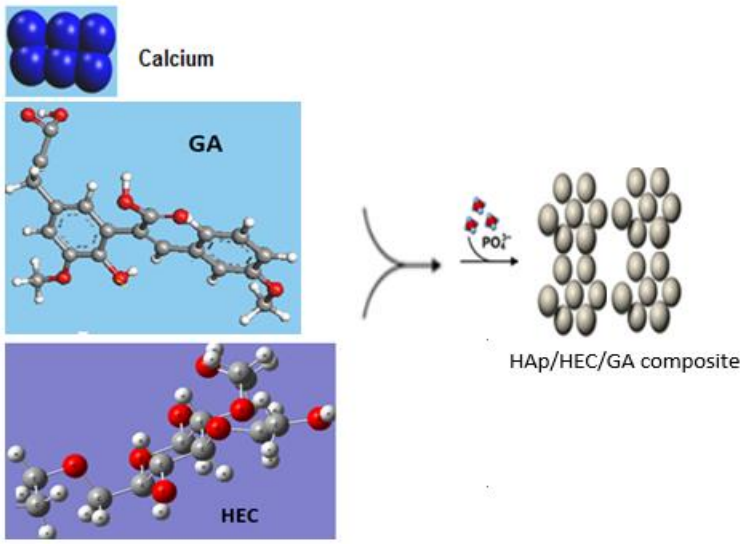

Figure 5. Proposed reaction route for the preparation of HAp / HEC / GA composites.

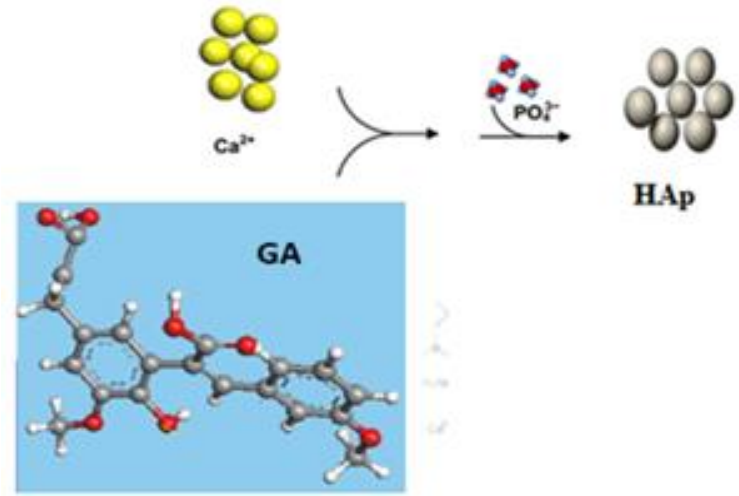

Figure 6. Proposed reaction route for the preparation of HApparticles in the presence of GA molecules

3.2 X-rays diffractions

The XRD patterns of the samples with different ratios show that these compounds maintain their apatite structure **Figure 7**. The GA influences the morphology of hydroxyapatite/hydroxyethyl cellulose but does not impact its crystallographic parameters. The x-ray diffraction analysis of the HApshows that the characteristic peaks are well compatible with JCPDS card, number 09-0432. The diffraction peaks, particularly, the (002), (211), (112) and (300) planes are high and narrow, which shows that the HAp is well crystallized **Figure 7**. **Figure 7** c-d shows the x-ray diffraction of the HAp/HEC/GA composites. A characteristic peak of the HApis observed at 2θ = 32° in the plane (211). This study illustrates the preparation of apatite materials with different sizes, which can be used as biomaterials due to their crystalline nature, comparable to that of bone, and their biocompatibility to calcified tissue.

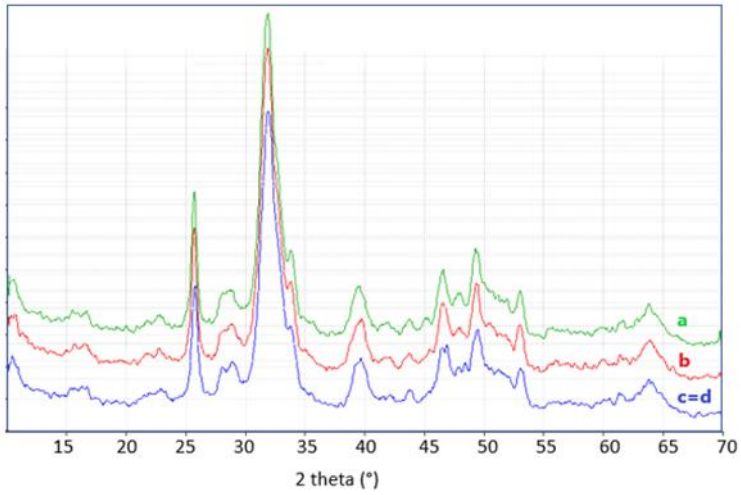

Figure 7. x-ray diffraction pattern of the HAp/HEC/GA composites. (a) 100/0/0, (b) 70/20/10, (c) 60/30/10, and (d) 50/40/10.

3.3 Scanning electron microscopy

Microstructure of composite based on HAp was characterized using SEM technique was performed under low accelerating voltage of 20 kV. Obtained images are presented in **Figure 8**. The micrographs indicate that the HEC/GA and HAp are composed of small spherical particles (images a and b). The SEM results of the HAp/HEC/GA composites show that the GA reduces the size of HApand HAp/HEC nanoparticles (images c and d). **Figure 9** shows the proposed model of the nature of the polymer/apatite matrix bond. A weak bond is observed between the OH group of GA and the OH of HEC and the Ca atom of HAp.

3.4 Antibacterial effect of HAp / HEC / GA composite

Figure 10 and **Table 1** show the antibacterial tests of the HAp-based composites. The HAp/HEC/GA (70/20/10) composite exhibits a significantly higher antibacterial activity, compared to the other composites tested separately, against four types of bacteria (S. aureus, B. cereus, P. aeruginosa, and E. coli). Their antibacterial potency is two times stronger than Streptomycin (control antibiotic), and about five times stronger than Ampicillin see **Table 1**.

Table 1 shows that all these composites present antifungal activities. The highest inhibition was observed for the HAp/HEC/GA (80/10/10) composite. The antimicrobial activities were selective for some composites, the HAp / HEC / GA (70/20/10) composite inhibits only the growth of the bacillus.

3.5 Atomic force microscopy

Atomic force microscopy (AFM) analysis was used to visualize and measuring surface rugosity with and without composite based of HAp. The AFM micrographs of the metallic surface with and without 1 g/L of HAp/HEC/GA composite are shown in **Figure 11**. In the presence of HAp/HEC/GA composite at the optimum concentration (1 g/L), the average rugosity was reduced to 1.3 µm, mainly due to the formation of a protective layer (Gopi *et al*., 2015).

DOI: https://doi.org/10.17509/ijost.v6i1.31480 |
p- ISSN 2528-1410 e- ISSN 2527-8045 |

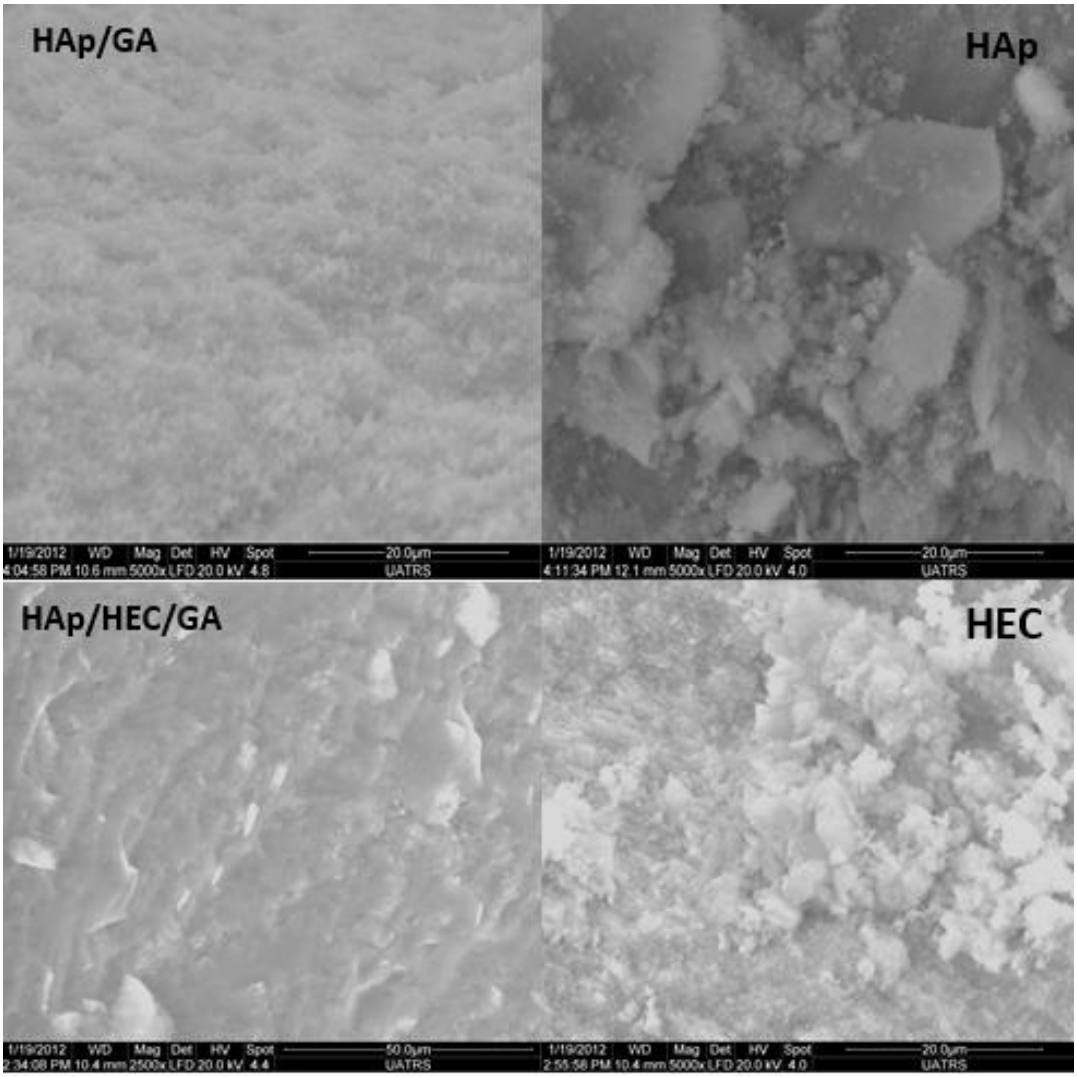

Figure 8. Scanning electron microscopy analysis of all HAp, HEC, GA and HAp/ HEC/GA composite.

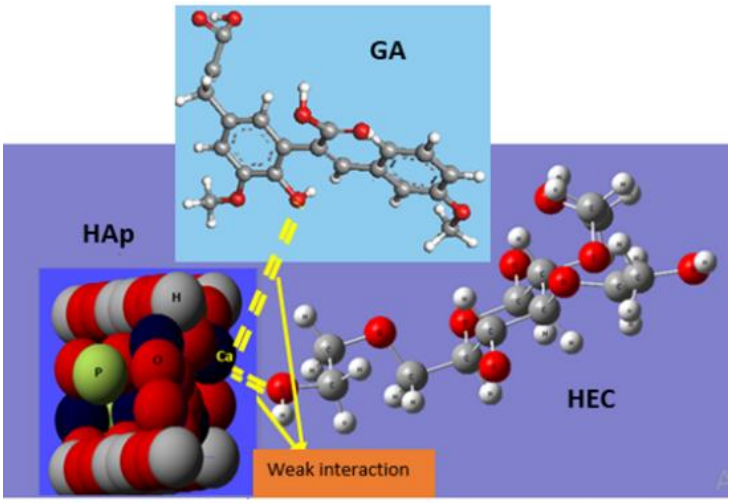

Figure 9. Schematic model of the bond between OH of HEC/ GA and Ca^{2+} of HAp.

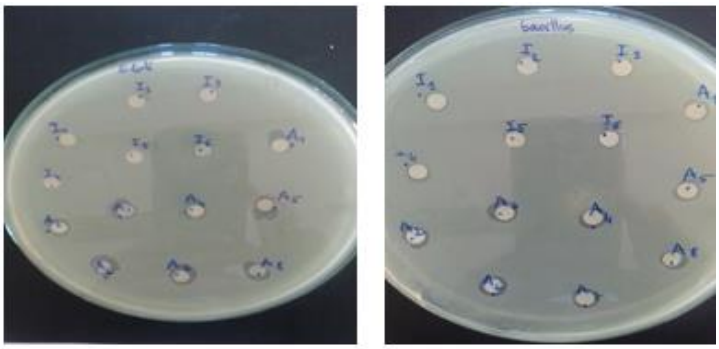

Figure 10. Antimicrobial test of the Hap-based composites.

Table 1. Inhibition diameter of three composites with positive and negative control tested on three bacteria and one fungus.

Stains	HAp/HEC/GA 80/10/10	HAp/HEC/GA 70/20/10	HAp/HEC/GA 60/30/10	C +	DMSO
B.S	9	9	9	26	-
M.L	9	-	-	27	-
E.coli	-	13	-	29	-
Candida	13	11	12	27	-

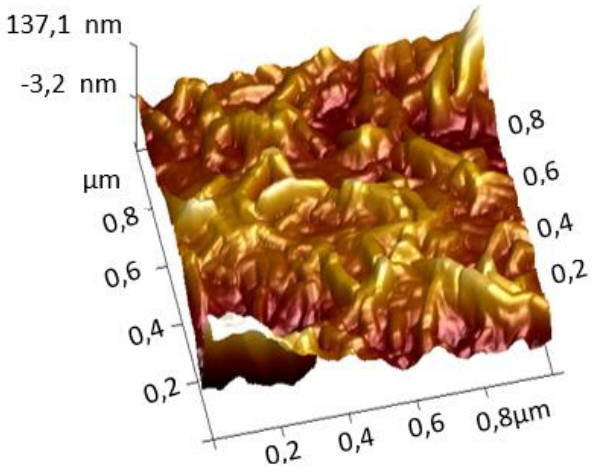

Figure 11. Atomic force microscopy AFM composite based of HAp/HEC/GA.

3.6 x-ray photoelectron spectroscopy

The growth of the organic inhibitor film and the adsorption of inhibitory compounds on the surface of the mild steel were performed by means of XPS. The investigations were carried out on the surface of the steel after 6 h of submersion in a solution of 1 M HCl containing 1 g/L of HAp/HEC/GA composite. The high resolution XPS spectrum for C1 of the base energy level spectrum for a mild steel surface in a 1M HCl

DOI: https://doi.org/10.17509/ijost.v6i1.31480 |
p- ISSN 2528-1410 e- ISSN 2527-8045 |

solution with HAp/HEC/GA composite can be divided into four distinct contributions **Figure 12**. Therefore, two different approaches were employed in the preparation of these composite particles. The surface chemistry of the three samples was studied by XPS **Figure 12**. C1 peak is divided into three components 287.8, 286.4, and 284.9 eV. The peaks indicate the O-C-O, C-OH and C-C bonds, and exist in chitosan **Figure 12A**. A third peak occur at 532.8 eV and Refers to the O1 attributed to the hydroxyl groups **Figure 12B**.

3.7 Metal ions removal

The removal of Zn^{2+} and Cu^{2+} on synthesis *HAp/ HEC/ GA* composite was investigated using a batch adsorption process which included suspension followed by filtration. the assessment of the filtrate allows determination of unrestricted ions. The adsorbent was suspended in the ion solution and shaken in a thermostatic bath. The effect of different parameters such as adsorbent dosage, time of removal, temperature, and pH were exploited to identify the best conditions for the highest adsorption efficiency. The analysis was carried out in glass containers (50 ml) which are placed in a shaking water bath. In order to measure the level of residual metal ions following any adsorption test, a portion from the mixture was collected by filtration through a 0.45 µm syringe filter and subjected to Flame Atomic Absorption, at 213.9 and 324.8 nm respectively. The amount of the metal ions adsorbed by the HAp/HEC/GA composite adsorbent qe (mg/g) and the adsorbent efficiency was determined using equations (1) and (2):

$$R\ (\%) = \frac{C_0 - C_e}{C_0}\ 100 \quad (1)$$

$$Q_e = \frac{C_0 - C_e}{m} V \quad (2)$$

where C_o is the initial concentration in ppm, C_e is the equilibrium concentration in ppm. V is the volume of aqueous phase (L), m is the mass of sorbent HAp/HEC/GA in mg. HAp(HAp), and Q_e (ppm) is the equilibrium adsorption capacity.

3.7.1 Optimum adsorbent dosage

In order to determine the optimal dosage corresponding to the lowest residual metal ion concentration, we performed the experiment at room temperature on 50 ml of each Cu^{2+} and Zn^{2+} ion using a concentration of 30 ppm, a pH of 6.3, and an adsorption time of 30 min. The influence of the adsorbent dose on the elimination of Cu^{2+} and Zn^{2+} ions is presented in **Figure 13A**. The absorbance of metal ions increased sharply until a dose of 2.0 mg/ml was reached and then stopped. This can be explained by the fact that the adsorption process is monitored by two mechanisms, diffusion and surface coordination. Consequently, as the adsorbent dose rises, the number of binding sites on the surface increases, therefore the removal efficiency increases. When all surface sites are covered, the process of diffusion begins, which is primarily governed by osmosis.

3.7.2 Effect of contact time

The adsorption of Cu^{2+} and Zn^{2+} metal ions by the composite base of the HAppolymer versus time was investigated at room temperature using conditions where the pH was 6.3, the starting concentration was 30 ppm, and the adsorbent dose was 2.0 mg/ml. **Figure 13B** shows that the adsorbed metal ions rapidly rising during the first 10 min as a result of the presence of coordination sites, then decrease in adsorption rate during the next 10 min. An equilibrium, he, is reached after 10 min, indicating that all coordination sites are occupied. A contact time of 15 min was selected as the optimum.

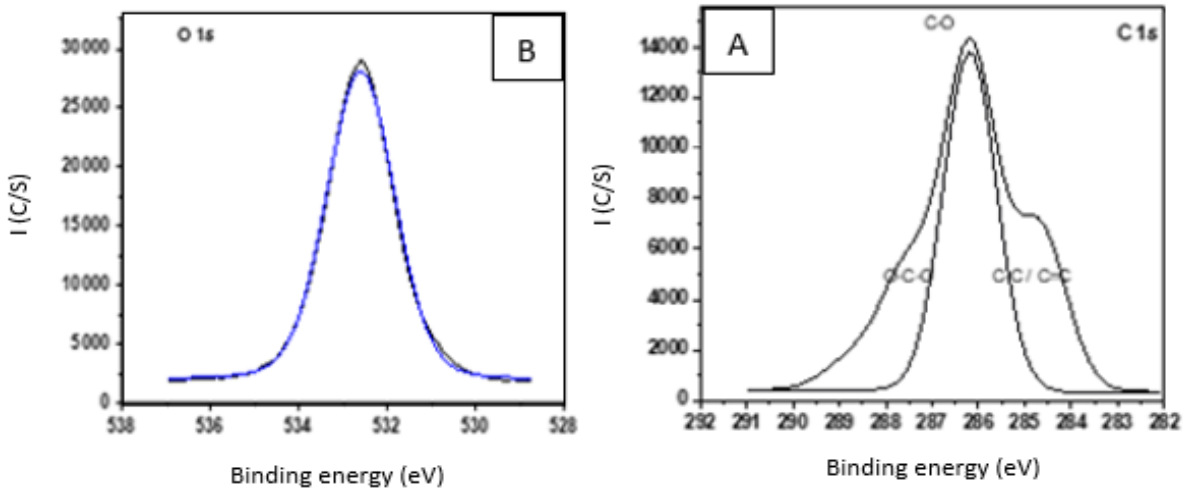

Figure 12. A) C 1s and B) O 1s base level of mild steel treated with HAp / HEC / GA.

3.7.3 Effect of pH

Figure 13C shows the influence of pH on the adsorption efficiency. The pH value is critical in adsorption, as it could be used to regulate the surface charge of the adsorbent.

The impact of pH on the adsorption of Cu^{2+} and Zn^{2+} metal ions by the composite based of HApsubstrates was also evaluated. The studies were carried out at 25 °C. The adsorption was evaluated over a pH range of 3.0–12. The results are summarized in **Figure 13C**. The highest efficiency for the removal of Cu^{2+} and Zn^{2+} from water was determined to be at pH 12. The per-centage of removal Cu^{2+} and Zn^{2+} at pH 12 was quantitative for HAp/HEC/GA. This could be because at high pH, the active sites on HEC/GA polymers are negatively partial negative charged, which means a high electron density causes a stronger dipole–dipole interaction between adsorbent and Cu^{2+} and Zn^{2+} cation. There also may be other types of adsorption involved such as ion exchange.

3.8 Adsorption analysis

Langmuir (equation 3) and Freundlich isotherm (equation 5) models were applied to investigate the adsorption equilibrium between Cu^{2+} and Zn^{2+} ion solution and the HAp / HEC / GA composite polymer (Laghzizil *et al*., 2001). Both models were used to assess the metal ion dispersion on the surface of the HAp/ HEC/GA composite once equilibrium is reached under constant temperature.

There are several isotherm models like Langmuir, Freundlich, etc. which can be applied at all temperatures. All of these models have equations that can be used, and the data will be fIt into these equations. One of the factors that can lead to the type of isotherm model is the correlation coefcients, R^2 (Gopi *et al*., 2008).

$$\frac{C_e}{Q_e} = \frac{1}{q_{max}} C_e + \frac{1}{q_{max} K_L} \quad (3)$$

Where C_e represents the equilibrium concentration of the adsorbate (mg/L), Qe is the amount of the adsorbate adsorbed per unit mass of HAp/HEC/GA composite at equilibrium (mg/g), q_{max} is the adsorption capacity equilibrium (mg/g), and K_L is is usually, the Langmuir afnity constant (L/mg).

From Langmuir isotherm model Some authors define the R_L ratio as a dimensionless

DOI: https://doi.org/10.17509/ijost.v6i1.31480 |
p- ISSN 2528-1410 e- ISSN 2527-8045 |

quantity indicating that sorption is favourable or not

$$R_L = \frac{1}{1 + K_L C_0} \quad (4)$$

Where C_o is the initial adsorbate concentration. If the value of R_L is higher than 1, this indicates that the adsorption is unfavorable. However, when the R_L value is between 1 and 0, this indicates favorable adsorption, whereas when R_L = 1 indicates the presence of linear adsorption.

The other type of isotherm model is Freundlich isotherm is an empirical formula which used for low concentrations and can be presented as (Gopi *et al.*, 2008):

$$\ln(q_e) = \ln k_F + \frac{1}{n} \ln Ce \quad (5)$$

where K_F is the Freundlich constant that deal with adsorption capacity (mg/g) and n is the heterogeneity coefficient which leads to how favorable the adsorption process (g/L).

Figure 14 summarizes all adjustment parameters. The correlation coefficients of the Freundlich isothermal model are lower than those of the Langmuir isothermal model **Table 2**, reflecting that the adsorption of Cu^{2+} and Zn^{2+} ions is in accordance with the Langmuir isothermal model, in which Cu^{2+} and Zn^{2+} cation are distributed equally and homogeneously across the porous surfaces of the HAp/HEC/GA composite.

The separation factor R_L, which has been calculated for different quantities of adsorbent, ranges from $0 < R_L < 1$ **Table 2**. This reflects the high degree of affinity of the HAp/HEC/GA composite for the studied metal ions.

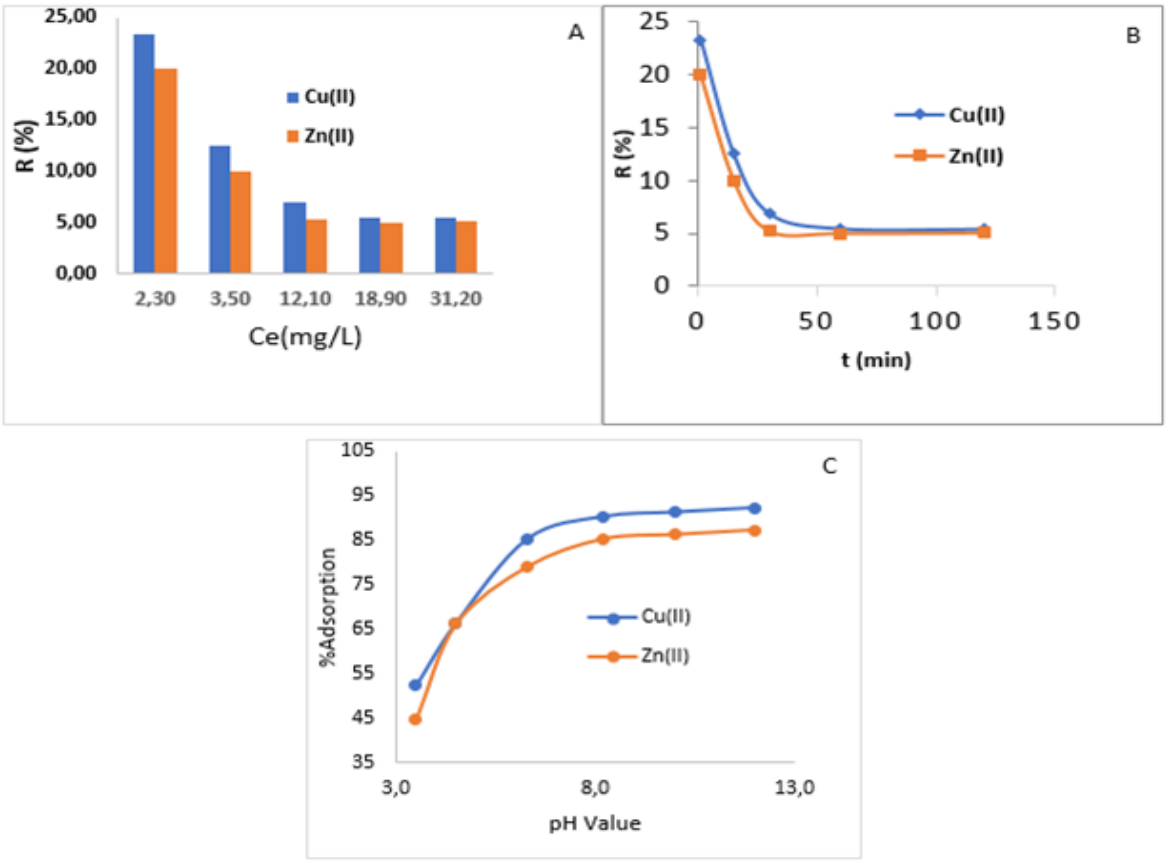

Figure 13. Effects of, **A**) Adsorbent dose **B**) Adsorption time, and **C**) pH on the metal removal.

3.9 Adsorption kinetics of Cu^{2+} and Zn^{2+} ions on HAp/HEC/GA composite

Presenting the experimental data through kinetics equations like the pseudo-first-order model, the pseudo-second-order model will describe the mechanism of adsorption of Cu^{2+} and Zn^{2+} ions in aqueous solution. Such studies give information about the possible mechanism of adsorption of Cu^{2+} and Zn^{2+} ions and different transition states on the final complex of Cu^{2+} and Zn^{2+} ions and the adsorbent. From the reactions parameters like rate constants and adsorption capacity factors, one can have an idea about the adsorption dynamics and this will help the industry for other applications.

The adsorption experimental data of Cu^{2+} and Zn^{2+} ions by the composite based of HApwere analyzed using the most common kinetic models to understand the nature of the adsorption process.

The adsorption of metals by solid adsorbents such as composite based of HApwas ftted to one of the most used kinetic models; pseudo-first order and pseudo-second order models, the equation can be written as the following. These kinetic models are shown in equations (7) and (8) (Gopi *et al*., 2009).

$$\ln(q_e - q_t) = \ln q_e - K_1 t \quad (7)$$

$$\frac{t}{q_t} = \frac{1}{K_{2q_e^2}} + \frac{t}{q_e} \quad (8)$$

Weber and Morris developed an equation describing the intraparticle diffusion and can be written as the following equation (9) (Gopi *et al*., 2009).

$$Q_t = K_{id} t^{1/2} + Z \quad (9)$$

where Q_t (mg g^{-1}) is adsorption capacity at any time t, k_{id} (mg/g $min^{1/2}$) is the intraparticle diffusion rate constant, and Z (mg/g) is a constant proportional to the thickness of the boundary layer.

Table 3 and **Figure 15** summarize the values of all parameters of the above equations. The plots of Ln (q_e-q_t) versus t **Figure 15 A-D** provide the value of K_1, whereas the values of K_2 and the adsorption capacity q_e were derived from the slope and intercept of the plot of t/Qt versus t **Figure 15 B-E**, while K_{id} and Z were deduced by tracing Qt vs $t^{1/2}$ **Figure 15 C-F**.

The experimental results show that the correlation coefficients (R^2) for the pseudo-second order kinetics model (0.91 to 0.973) is greater than the pseudo-first order (0.891). A further indication was also provided by the calculated qe values (2.675, 15.252, 20.856 mg / g) which are similar to the experimental qe values (2.133, 13.91, 18.786 mg / g) for the pseudo-second order model suggesting that the process of adsorption of Zn and Cu on the surfaces of the HAp / HEC / GA composite polymer corresponds to the pseudo-second order **Table 3 and Figure 15B -E**.

From **Figure 15C-F** (Qt *vs.* $t^{1/2}$) K_{id} and Z were calculated and reported in **Table 3**. All graphs plotted in **Figure 15** are straight line and didn't cross the origin, indicating the occurrence of more than one rate-limiting process.

Based on initial graphs linearity presented in **Figure 15 B-E** we can conclude that, at the outset of the adsorption process, the adsorption of Cu^{2+} and Zn^{2+} on the HAp / HEC / GA composite takes place initially by an instantaneous adsorption step (on the external surface), which caused a chemical complexation between the metal ions and OH and further functionalities (Gopi, 2012; Azzaoui, 2017). The other steps were also linear, showing a progressive adsorption of Cu^{2+} and Zn^{2+} ions and the step of limiting intraparticle diffusion rate.

The results presented in **Table 3** reveal that the Z values reflect an expansion in the upper layer and a decrease in the outer mass

DOI: https://doi.org/10.17509/ijost.v6i1.31480 |
p- ISSN 2528-1410 e- ISSN 2527-8045 |

transfer although the inner mass transfer potential was increasing. The energy of activation of the adsorption process was computed at 298 and 323K according to Equation 9.

These findings are important for understanding how temperature influences adsorption performance of Cu^{2+} and Zn^{2+} ions on the HAp / HEC / GA composite. The activation energy computed was nearly zero, suggesting a spontaneous adsorption process.

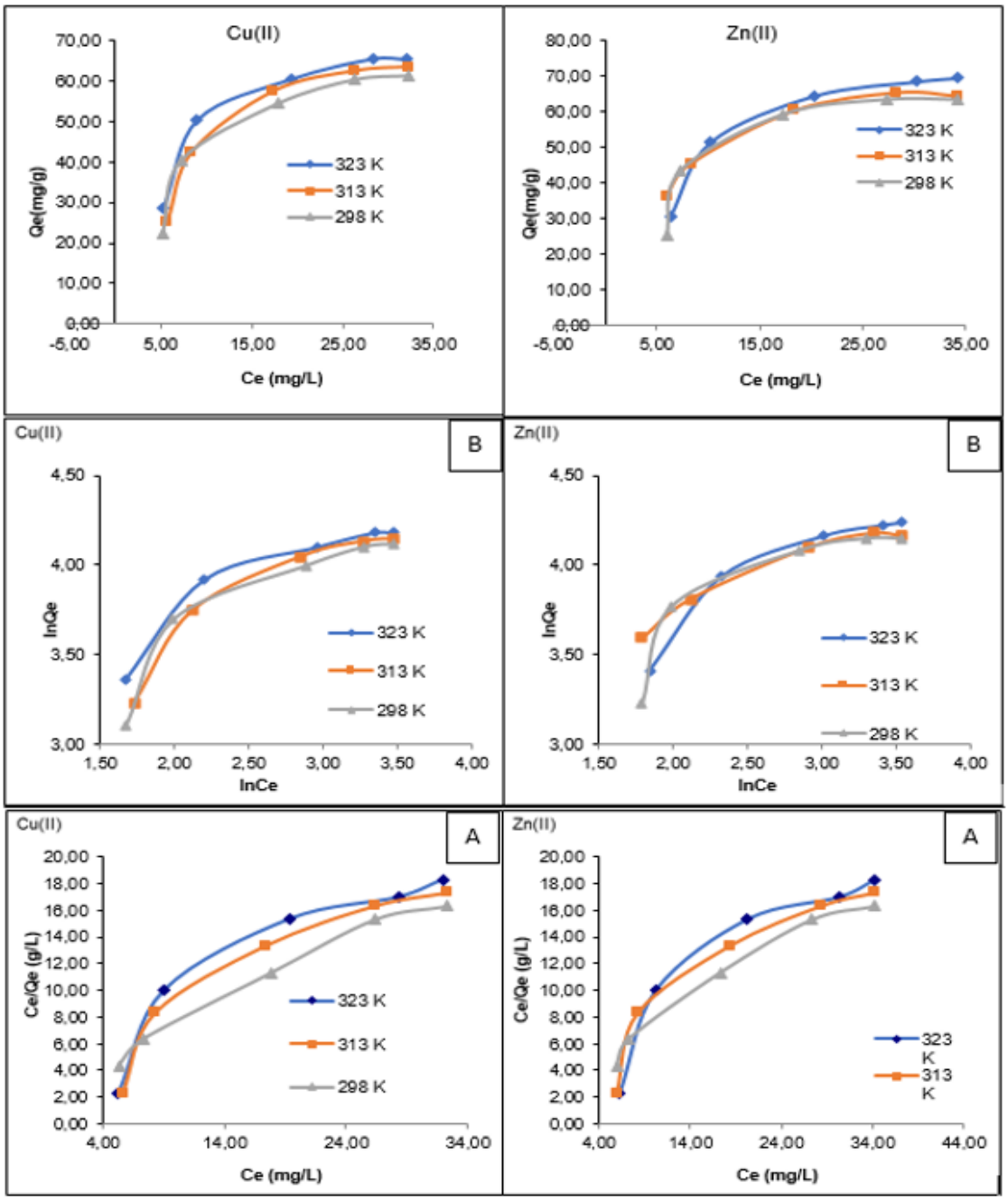

Figure 14. A) Langmuir adsorption model and **B)** Freundlich adsorption model of Cu^{2+} and Zn^{2+} ions on HAp/HEC/GA composite at different temperatures

3.10 Thermodynamics study

In this study, different parameters were calculated like the standard free energy, standard enthalpy, and standard entropy. The aim of this study is to understand spontaneity and to understand the nature of adsorption. The following equation was used (Gopi *et al*., 2009):

$$K_c = C_{ads}/C_e \quad (11)$$

$$\Delta G^0 = -RT\ln K_c \quad (12)$$

$$\ln K_s = \frac{\Delta S}{R} - \frac{\Delta H}{RT} \quad (13)$$

where K_c is an apparent constant of the thermodynamics; and C_{ads} and C_e are respectively the amount adsorbed at equilibrium (mg/L) and concentration of metal ion in the solution (mg/L), R is the universal gas constant (8.314J/mol K); T is the solution temperature. The (ΔG^0) (J mol^{-1}) value was determined according to equation 12. The ln K_s *vs.* 1/T was mapped as illustrated in **Figure 16**, the slopes and crossings were utilized to determine various thermodynamics parameter as shown in **Table 3**.

The value obtained for ΔS^0 and ΔH^0 are positive, whereas the entropy raised at the solid/solution interface induced as a result of the adsorption process. The findings further indicate that, all free energies for the HAp/HEC/GA composite were negative reflecting a spontaneous process of adsorption at various temperatures.

The metal removal mechanism by adsorption generally occurs at various stages. In the first step, metal ions migrate from most of the solution to the outer surface of the HAp / HEC / GA composite, then diffuse across the boundary-layer to the outer surface of the HAp / HEC / GA composite, followed by adsorption of metals ions at active sites on the HAp / HEC / GA composite surface, and lastly, intra-particle diffusion and adsorption of ions across the HAp / HEC / GA composite particles. Consequently, the sorption mechanism was investigated using the liquid film model and the intra-particle diffusion model.

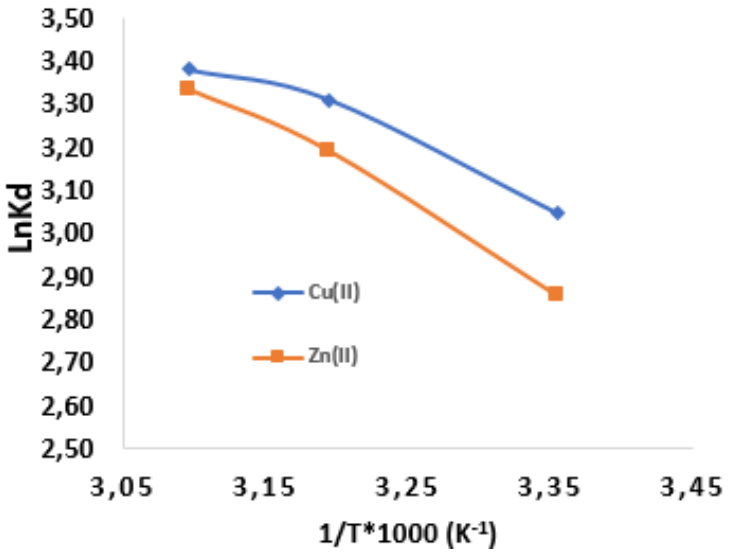

Figure 16. Adsorption thermodynamics of Cu^{2+} and Zn^{2+} ions onto HAp/HEC/GA composite

DOI: https://doi.org/10.17509/ijost.v6i1.31480 |
p- ISSN 2528-1410 e- ISSN 2527-8045 |

The model of liquid film diffusion implies that the flow of adsorbate particles through a liquid film around the solid adsorbent is the longest phase in the adsorption process (i.e., the one that determines the kinetics of the velocity processes). The equation (10) describes the liquid film diffusion model.

$$\text{Ln}\ (1 - F) = k_{fd}\ t \qquad (10)$$

where F is the ratio ($F = q_t/q_e$) reached at the equilibrium, and k_{fd} (min^{-1}) is the film-diffusion coefficient. A linear plot of ln(1–F) versus t, at zero intercept, involve that the kinetics of the adsorption process is controlled by the diffusion across the liquid film enclosing the HAp/HEC/GA composite. q_e is the adsorption capacity at equilibrium ($mg.g^{-1}$). **Figure 17** highlighted that, using the liquid film diffusion model to the analytical results of Cu^{2+} and Zn^{2+} adsorption by the HAp / HEC / GA composite from aqueous solution at various temperatures did not converge, didn't exhibit linear lines crossing the origin, and had very low correlation coefficients: 0.1876 and 0.1578 for Cu^{2+} and Zn^{2+}, respectively. This suggests that diffusion of ions through the liquid film around the HAp / HEC / GA composite was not the step that determines the velocity. It should be noted that the liquid film diffusion model was used at the first few points during 10 min of adsorption, and the coefficients of regression were modestly enhanced to 0.9735 and 0.9873 for Cu^{2+} and Zn^{2+}, respectively. These results suggest that the diffusion pattern of the liquid film is not the slowest step to determine the rate, but could affect the adsorption process, particularly at the commencement of adsorption, as indicated in **Table 3.**

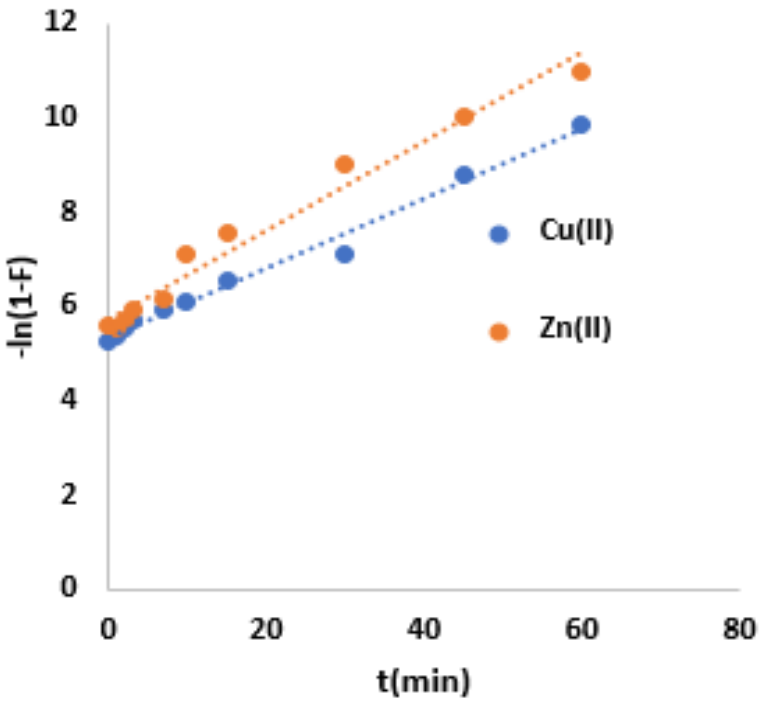

Figure 17. Liquid film diffusion model plots for the adsorption of composite based of HAp/HEC/GA composite

4. CONCLUSION

Composite consisting of HAp/HEC/GA could be developed synthetic method to obtain bone substitute material. This HAp/HEC/GA nanocomposite was synthesized using reprecipitation method by which the samples were mixed. This method made the mixture more homogeneous and the final product was isolated by filtration. This new product is an addition to the family of composites for medical and environmental use. The antibacterial and antifungal testing showed a moderate inhibition for the HAp/HEC/GA (80/10/10) composite against gram positive and gram negative bacteria.

The application of the Langmuir and Freundlich equations on the experimental data showed that, the Langmuir isotherm model fitted well the experimental data for the adsorption of Cu^{2+} and Zn^{2+} onto the HAp/ HEC/GA composites. Various kinetic models were also used to explain the adsorption mechanism. The data indicated that the adsorption of Cu^{2+} and Zn^{2+} onto HAp/ HEC/GA best fit a pseudo-second-order kinetic mechanism. The adsorption of Cu^{2+} and Zn^{2+} ions onto the composites occurred preferentially at neutral pH value. These results indicate that the Cu^{2+} and Zn^{2+} ions were most likely adsorbed onto uncharged sites on the composites surfaces such as amine and hydroxyl groups. Thermodynamics study showed that the adsorption is spontaneous and exothermic with physisorption nature of the adsorption process.

5. ACKNOWLEDGMENTS

The authors would like to thank both the Department of Plant and Soil Science, Texas Tech University, Lubbock, TX, USA, Plant Biotechnology Laboratory “BiotecV”. Laayoune Higher School of Technology, Laayoune. Ibn Zohr University, Morocco, Laboratory of Plant Biotechnology and the department of chemistry at Mohammed Premier University for their help with sample characterization.

5. AUTHORS’ NOTE

The authors declare that there is no conflict of interest regarding the publication of this article. Authors confirmed that the paper was free of plagiarism.

6. REFERENCES

Aliabadi, M., Irani, M., Ismaeli, J. and Najafzadeh, S. (2014). Design and evaluation of chitosan/HApcomposite nanofiber membrane for the removal of heavy metal ions from aqueous solution. *Journal of the Taiwan Institute of Chemical Engineers*, *45*(2), 518-526.

Azzaoui, A, K., Lamhamdi, A., Mejdoubi, E., Hammouti, B., and Berrabah, M. (2014). Synthesis of hydroxyethylcellulose and hydroxyapatite nanocompositefor analysis of bisphenol. *Arabian Journal of Chemical and Environmental Research*, *2*(2014), 41–48.

Azzaoui, K., Berrabah, M., Mejdoubi, E., Lamhamdi, A., Elidrissi, A., and Hammouti, B. (2014). Use of hydroxylapatite composite membranes for analysis of bisphenol a. *Research on Chemical Intermediates*, *40*(8), 2621-2628.

Azzaoui, K., Lamhamdi, A., Mejdoubi, E., Berrabah, M., ELidrissi, A., Hammouti, B., Zaoui, S., and Yahyaoui. R. (2013). Synthesis of nanostructured hydroxyapatite in presence of

polyethylene glycol 1000. *Journal of Chemical and Pharmaceutical Research*, *5*(12), 1209-1216.

Azzaoui, K., Lamhamdi, A., Mejdoubi, E., Berrabah, M., Hammouti, B., Elidrissi, A., and Al-Deyab, S. S. (2014). Synthesis and characterization of nanocompositebased on cellulose acetate and hydroxyapatite application to the absorption of harmful substances. *Carbohydrate Polymers*, *111*(2014), 41–46.

Azzaoui, K., Mejdoubi, E., Jodeh, S., Lamhamdi, A., Rodriguez-Castellón, E., Algarra, M., and Lgaz, H. (2017). Eco friendly green inhibitor Gum Arabic (GA) for the corrosion control of mild steel in hydrochloric acid medium. *Corrosion Science*, *129*(2018), 70-81.

Azzaoui, K., Mejdoubi, E., Lamhamdi, A., Hammouti, B., Akartasse, N., Berrabah, M., and Abidi, N. (2016). Novel tricomponenets composites films from polylactic acid/hydroxyapatite/poly-caprolactone suitable for biomedical applications. *Journal of Materials and Environmental Science*, *7*(3), 761-769.

Azzaoui, K., Mejdoubi, E., Lamhamdi, A., Zaoui, S., Berrabah, M., Elidrissi, A., and Al-Deyab, S. S. (2015). Structure and properties of hydroxyapatite/hydroxyethyl cellulose acetate composite films. *Carbohydrate Polymers*, *115*(2015), 170-176.

Azzaoui, K., Hammouti, B., Lamhamdi, A., Mejdoubi, E., and Berrabah, M. (2015). The Gum Arabic in the southern region of Morocco. *Moroccan Journal of Chemistry*, *3*(1), 99-107.

Banerjee, S. S., and Chen, D. H. (2007). Fast removal of copper ions by gum arabic modified magnetic nano-adsorbent. *Journal of Hazardous Materials*, *147*(3), 792-799.

Banerjee, K., Amy, G. L., Prevost, M., Nour, S., Jekel, M., Gallagher, P. M., and Blumenschein, C. D. (2008). Kinetic and thermodynamic aspects of adsorption of arsenic onto granular ferric hydroxide (GFH). *Water Research*, *42*(13), 3371-3378.

Carabante, I., Grahn, M., Holmgren, A., Kumpiene, J., and Hedlund, J. (2009). Adsorption of as (V) on iron oxide nanoparticle films studied by in situ ATR-FTIR spectroscopy. *Colloids and Surfaces A: Physicochemical and Engineering Aspects*, *346*(1-3), 106-113.

Chen, A. H., Liu, S. C., Chen, C. Y., and Chen, C. Y. (2008). Comparative adsorption of Cu (II), Zn (II), and Pb (II) ions in aqueous solution on the crosslinked chitosan with epichlorohydrin. *Journal of Hazardous Materials*, *154*(1-3), 184-191.

Corami, A., D'Acapito, F., Mignardi, S., and Ferrini, V. (2008). Removal of Cu from aqueous solutions by synthetic hydroxyapatite: EXAFS investigation. *Materials Science and Engineering B*, *149*(2), 209-213.

Corami, A., Mignardi, S., and Ferrini, V. (2007). Copper and zinc decontamination from single- and binary- metal solutions using hydroxyapatite. *Journal of Hazardous Materials*, *146* (1-2), 164-170.

Destainville, A., Champion, E., Bernache-Assollant, D., and Laborde, E. (2003). Synthesis, characterization and thermal behavior of apatitic tricalcium phosphate. *Materials Chemistry and Physics*, *80*(1), 269-277.

Dhillon, A., and Kumar, D. (2017). Dual adsorption behaviour of fluoride from drinking water on Ca-Zn$(OH)_2CO_3$ adsorbent, *Surfaces and Interfaces, 6*, 154–161.

Dhillon, A., Sharma, T. K., Soni, S. K., and Kumar, D. (2016). Fluoride adsorption on a cubical ceria nanoadsorbent: function of surface properties. *RSC Advances*, *6*(92), 89198-89209.

Dhillon, A., Soni, S. K., and Kumar, D. (2017). Enhanced fluoride removal performance by Ce–Zn binary metal oxide: adsorption characteristics and mechanism. *Journal of Fluorine Chemistry*, *199*(2017), 67-76.

Eddy, N., O., Ameh, P. O., Victor, O., and Odiongenyi, A. O. (2014). Chemical information from GCMS and FTIR Studies on ficusthonningii gum and its potential as a corrosion Inhibitor for aluminium in acidic medium. *International Journal of Chemical, Material and Environmental Research, 1*(1), 3-15.

Elliott J.C., Mackie P.E., Young RA. (1973). Monoclinic hydroxyapatite. *Science, 180*(4090), 1055–1057.

Gandhi, M. R., Kousalya, G. N., and Meenakshi, S. (2011). Removal of copper (II) using chitin/chitosan nano-hydroxyapatite composite. *International Journal of Biological Macromolecules*, *48*(1), 119-124.

Gao, Y., and Mucci, A. (2001). Acid base reactions, phosphate and arsenate complexation, and their competitive adsorption at the surface of goethite in 0.7 M NaCl solution. *Geochimica et Cosmochimica Acta*. *65*(14), 2361–2378.

Goldberg, S. (1985). Chemical modeling of anion competition on goethite using the constant capacitance model. *Soil Science Society of America Journal*, *49*(4), 851-856.

Goldberg, V., and Johnstony, C. T. (2001). Mechanisms of arsenic adsorption on amorphous oxides evaluated using macroscopic measurements, vibrational spectroscopy, and surface complexation modeling. *Journal of Colloid and Interface Science*, *234*(1), 204–216.

Gopi, D., Govindaraju, K. M., Victor, C. A. P., Kavitha, L., and Rajendiran, N. (2008). Spectroscopic investigations of nanohydroxyapatite powders synthesized by conventional and ultrasonic coupled sol–gel routes. *Spectrochimica Acta Part A: Molecular and Biomolecular Spectroscopy*, *70*(5), 1243-1245.

Gopi, D., Indira, J., Prakash, V. C. A., and Kavitha, L. (2009). Spectroscopic characterization of porous nanohydroxyapatite synthesized by a novel amino acid soft solution freezing method. *Spectrochimica Acta Part A: Molecular and Biomolecular Spectroscopy*, *74*(1), 282-284.

Gopi, D., Kanimozhi, K., and Kavitha, L. (2015). Opuntia ficus indica peel derived pectin mediated hydroxyapatite nanoparticles: Synthesis, spectral characterization, biological and antimicrobial activities. *Spectrochimica Acta Part A: Molecular and Biomolecular Spectroscopy*, *141*(2015), 135-143.

DOI: https://doi.org/10.17509/ijost.v6i1.31480 |
p- ISSN 2528-1410 e- ISSN 2527-8045 |

Gopi, D., Nithiya, S., Shinyjoy, E., and Kavitha, L. (2012). Spectroscopic investigation on formation and growth of mineralized nanohydroxyapatite for bone tissue engineering applications. *Spectrochimica Acta Part A: Molecular and Biomolecular Spectroscopy*, *92*(2012), 194-200.

Grossl, P. R., Eick, M., Sparks, D. L., Goldberg, S., and Ainsworth, C. C. (1997). Arsenate and chromate retention mechanisms on goethite. 2. Kinetic evaluation using a pressure-jump relaxation technique. *Environmental Science and Technology*, *31*(2), 321-326

Hamed, O., Lail, B. A., Deghles, A., Qasem, B., Azzaoui, K., Obied, A. A., Algarra, M., and Jodeh, S. (2019). Synthesis of a cross-linked cellulose-based amine polymer and its application in wastewater purification. *Environmental Science and Pollution Research*, *26*(27), 28080-28091.

Jain, A., Raven, K. P., and Loeppert, R. H. (1999). Arsenite and arsenate adsorption on ferrihydrite: Surface charge reduction and net OH-release stoichiometry. *Environmental Science and Technology*, *33*(8), 1179-1184.

Kamnev, A. A., Colina, M., Rodriguez, J., Ptitchkina, N. M., and Ignatov, V. V. (1998). Comparative spectroscopic characterization of different pectins and their sources. *Food Hydrocolloids*, *12*(3), 263-271.

Kmita, A., Ślósarczyk, A., and Paszkiewicz, Z. (2006). Mechanical properties of HAp–ZrO2 composites. *Journal of the European Ceramic Society*, *26*(8), 1481-1488.

Laghzizil, A., Mekkaoui, M., Ferhat, M., and Barboux, P. (2001). Sorption study of tribenuron-methyl onto apatite minerals. *Toxicological and Environmental Chemistry, 81*(1-2), 9-15.

Lamhamdi, A., Azzaoui, K., Mejdoubi, E., Garoiz, H., Berabah, M., Elbali, B., and Hammouti, B. (2014). Contribution of adsorption of metals using calcium phosphates in the presence of support polyethylene glycol. *Mor J Chem*, *2*(2), 90-96.

Lamm, S. H., Engel, A., Kruse, M. B., Feinleib, M., Byrd, D. M., Lai, S., and Wilson, R. (2004). Arsenic in drinking water and bladder cancer mortality in the United States: An analysis based on 133 US counties and 30 years of observation. *Journal of Occupational and Environmental Medicine*, *46*(3), 298-306.

Lee, Y. J., Elzinga, E. J., and Reeder, R. J. (2005). Sorption mechanisms of zinc on hydroxyapatite: systematic uptake studies and EXAFS spectroscopy analysis. *Environmental Science and Technology*, *39*(11), 4042-4048.

LI, D.X., Hou, W. G., Li, S. P., Hao, M. T., and Zhang, G. Y. (2004). The isoelectric point and the points of zero charge of Fe-Al-Mg Hydrotalcite-like compounds. C*hinese Chemical Letters, 15*(2), 224 – 227.

Lin, L., Jing, C., Jian, H., Yurong, C., and Juming, Y. (2010). Extraction of pectins with different degrees of esterification from mulberry branch bark. *Bioresource Technology, 101*(9), 3268–3273.

Luong, N. D., Moon, I. S., Lee, D. S., Lee, Y. K., and Nam, J. D. (2008). Surface modification of poly (l-lactide) electrospun fibers with nanocrystal hydroxyapatite for engineered scaffold applications. *Materials Science and Engineering: C*, *28*(8), 1242-1249.

Pivarciova, L., Rosskopfova, O., Galambos, M., and Rajec, P. (2014). Adsorption behavior of Zn(II) ions on synthetic hydroxyapatite. *Desalination and Water Treatment*, *55*(7), 1825-1831.

Roque, A. C. A., and Wilson Jr, O. C. (2008). Adsorption of gum Arabic on bioceramic nanoparticles. *Materials Science and Engineering: C*, *28*(3), 443-447.

Sandip, M., Manoj, K. S., and Raj, K. P. (2013). Adsorption studies of arsenic (III) removal from water by zirconium polyacrylamide hybrid material (ZrPACM-43). *Water Resources and Industry, 4*(2013), 51–67.

Sulastri, A. and Rahmidar, L. (2016). Fabrication of biomembrane from banana stem for lead removal. *Indonesian Journal of Science and Technology, 1*(1), 115-131

Tabaght, F. E., Azzaoui, K., Elidrissi, A., Hamed, O., Mejdoubi, E., Jodeh, S., Akartasse, N., Lakrat, M., and Lamhamdi, A. (2019). New nanostructure based on hydroxyapatite modified cellulose for bone substitute, synthesis, and characterization. *International Journal of Polymeric Materials and Polymeric Biomaterials, 1*(2), 1-12.

Takeuchi, Y., Suzuki, T., and Arai, H. (1988). A study of equilibrium and mass transfer in processes for removal of heavy-metal ions by hydroxyapatite. *Journal of Chemical Engineering of Japan*, *21*(1), 98-100.

Xiaoguang, C. M., Liu, S., Baidas, S., Patraju, R., Christodoulatos, C., and Korfiatis, G. P. (2005). Surface complexation of organic arsenic on nanocrystalline titanium oxide. *Journal of Colloid and Interface Science, 290*(1), 14–21.

Yin, G., Liu, Z., Zhan, J., Ding, F., and Yuan, N. (2002). Impacts of the surface charge property on protein adsorption on hydroxyapatite. *Chemical Engineering Journal*, *87*(2), 181-186.

Zhang, S., and Gonsalves, K. E. (1997). Preparation and characterization of thermally stable nanohydroxyapatite. *Journal of Materials Science: Materials in Medicine*, *8*(1), 25-28.

DOI: https://doi.org/10.17509/ijost.v6i1.31480 |
p- ISSN 2528-1410 e- ISSN 2527-8045 |